

Tricontinuous mesophases of balanced three-arm 'star polyphiles'

Stephen T. Hyde,^a Liliana de Campo^a and Christophe Oguey^b

Received 18th December 2008, Accepted 24th April 2009

First published as an Advance Article on the web 9th June 2009

DOI: 10.1039/b822814k

We construct simple models to compare ordered tricontinuous patterns that are topologically consistent with the constraints imposed by three-arm star polyphile self-assembly, analogous to steric packing and elastic bending models used to analyse bicontinuous mesophases in amphiphilic assemblies. We find a number of competing low-energy ordered structures, composed of threading of three identical labyrinths, with three-fold infinite branch lines, that are likely to be of comparable energy for polyphile shapes with moderately splayed arms. These patterns are triply-periodic analogues of the hexagonal honeycomb, which is most favoured for unsplayed three-arm polyphile architectures.

1 Introduction

Amphiphiles self-assemble to segregate hydrophobic and hydrophilic species. A number of mesophases form in solution. Ordered bicontinuous phases are well described by the geometry of triply-periodic minimal surfaces, which relate the amphiphilic bilayer geometry to a local molecular shape, set by a balance of repulsive interactions between hydrophilic head-groups and segregation of hydrophobic chains, driven by the hydrophobic effect. The phenomenon of bicontinuous mesostructures is essentially reduced to one of finding homogeneous partitions of space into domains separated by hyperbolic interfaces of nearly constant curvatures in order to minimise the membrane bending energy. Optimal solutions are the lowest genus (3), symmetric triply-periodic minimal surfaces formed in three-dimensional euclidean space, namely the *D*, *gyroid* and *P* surfaces. The striking long-range crystallinity of these structures is a response to the demand for curvature homogeneity in pure amphiphilic systems, since aperiodic, singly- or doubly-periodic minimal surfaces are likely to carry larger curvature deviations and incur a heavier bending-energy cost. The same structures also emerge in copolymer assemblies, driven by the requirement to segregate copolymer blocks with high mixing energies (or large Flory–Huggins, χ , parameters). Here the self-assembly is driven by the surface tension between the immiscible blocks, in concert with a requirement to retain high configurational entropy of the copolymer chains.

A similar variety of patterns has been observed in solid mesoporous materials grown in aqueous surfactant systems under various conditions. The structures of these solid materials are accessible to more detailed probes than those available for soft materials, and electron microscopy techniques have led to detailed high-resolution structural analyses that confirm the relevance of the *gyroid* and *D* surfaces as useful models for bicontinuous mesoporous materials.^{1,2} Very recently, the formation of an entirely novel 'tri-continuous' mesoporous

material has been reported, whose silica walls trisect space into three interwoven channel systems.³ The possibility of this new class of structures arising in soft molecular systems has been discussed in theoretical studies of patterns containing three-fold interpenetrating channels.^{4–6} Here we explore the possible formation of these tricontinuous patterns in novel 'polyphilic' molecular systems, that are more complex than amphiphiles. Our interest in polyphilic systems was piqued by early studies of complex copolymer molecules, which suggested very complex mesostructures, possibly with three interwoven 3D domains.⁷ Copolymer science has now moved beyond just two immiscible domains: so-called 'mikto-arm' copolymers have been investigated, containing three and four mutually immiscible domains, joined to a common central node, forming a star architecture. The problem of self-assembly in these systems is more challenging than that of two-phase systems, since all three (or more) moieties share a common molecular centre from which the immiscible moieties radiate. These studies confirm the presence of 'branch-lines' in ordered assemblies, which define edges shared by all domain types, described in more detail below. Previous works have demonstrated that these systems form a plethora of ordered mesophases, driven by segregation of the multiple moieties into isolated domains. A number of experimental studies of three- and four-arm mikto copolymer melts have confirmed the formation of discrete domains, separated by two-phase walls and three- or four-phase lines.^{8–19}

To date, nearly all reported mesostructures – with the notable exception of ref. 7 discussed above – are (somewhat idealised) prismatic arrays made of extended rod-shaped domains, separated by planar interfaces, with molecular junctions lying on extended, uncurved three- or four-fold branch lines. The simplest structure is the usual hexagonal honeycomb, illustrated in Fig. 1, with a 2D hexagonal array of triple-lines, defining the loci of copolymer central nodes, common to three distinct hexagonal domains, extended along the third direction. Theoretical studies support these findings. Lattice model simulations by Dotera and colleagues produced mesostructures formed by extending various tilings of the flat plane into the third dimension under pure translation normal to the plane, giving extended prismatic domains (just as the hexagonal honeycomb is related to the hexagonal tiling of the plane). These planar tilings include most

^aApplied Mathematics, Research School of Physical Sciences, Australian National University, Canberra, Australia. E-mail: stephen.hyde@anu.edu.au; liliana.decampo@anu.edu.au

^bLPTM, CNRS UMR 8089, Université de Cergy-Pontoise, 2 Avenue Adolphe Chauvin, 95302 Cergy-Pontoise, France. E-mail: oguey@ptm.u-cergy.fr

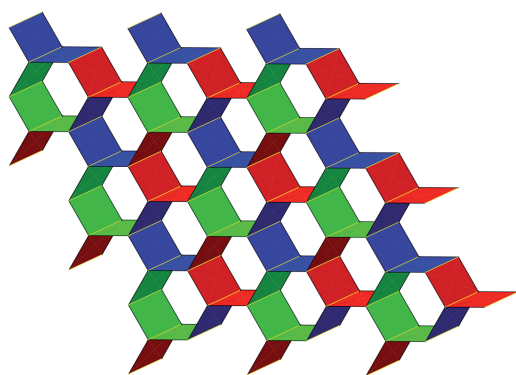


Fig. 1 Slice of the hexagonal honeycomb, the simplest spatial pattern that can be realised by three-arm star polyphiles. The prism walls separate distinct domains (coloured red, green and blue). Polyphile molecular junctions that link all three arms lie on the three-fold branch lines (marked in yellow).

Archimedean tilings,^{20–22} as well as quasi-crystalline patterns.²³ Huang *et al.* have implemented dissipative particle dynamics techniques to explore mikto-arm self-assembly as a function of the interactions between the molecular species making up the mikto-arm copolymers.²⁴ Their work also supports the presence of prismatic domains, whose cross-sections are planar tilings, and further suggests the possibility of topologically complex sponge-like microdomains, intergrown with various compact (closed) domain shapes. It is therefore clear that star-shaped mikto-arm copolymers, whose arms are sufficiently mutually immiscible, indeed form a variety of liquid-crystalline structures.

Until now, little attention has been paid to the possibility of self-assembly of lower molecular weight molecules whose arms are *oligomeric* rather than *polymeric*. We have synthesised a number of examples of these *star polyphiles*, defined as star-shaped molecules with three or more immiscible oligomeric chains (*e.g.* C_i hydrocarbon chains, C_j fluorocarbon chains and polyoxyethylene chains, PEO_k , $i, j, k < 16$) linked to a common node (*e.g.* tri-substituted phloroglucinol).²⁵ Just as copolymers may be viewed as polymeric analogues of amphiphiles, star-shaped mikto-copolymers are analogues of star polyphiles. We have found a number of liquid-crystalline mesophases of these polyphiles whose stability depends on temperature and the presence and type of solvents (with up to three mutually immiscible solvents: water, fluorocarbon and hydrocarbon). The various mesostructures are still being determined. These materials display some features of thermotropic and lyotropic liquid-crystalline materials formed by amphiphiles in solution, however, in contrast to amphiphilic systems and like mikto-arm copolymers, polyphile assemblies are expected to contain multi-phase *lines* as well as two-phase *interfaces*. Recent coarse-grained simulations, based on the ESPResSO software package²⁶ suggest a suite of possible structures, including the planar tilings seen in mikto-arm copolymers systems.²⁷ In addition, complex intergrowths of three interwoven sponge-like domains have been observed in these simulations, forming novel *tricontinuous* patterns, that we will explore in detail in this paper.²⁸ To our knowledge, these structures have been reported in only one preliminary study of mikto-arm copolymeric materials.⁷ We

suspect that their rarity to date is likely to be due to their structural complexity, making them difficult to identify, rather than any intrinsic feature that precludes their formation in mikto-arm copolymers. We construct a simple model of polyphile molecular shape and the resulting self-assemblies, focusing in particular on tricontinuous self-assemblies. This paper is motivated by our interest in forming these phases and the most appropriate molecular designs to yield tricontinuous patterns from self-assembled polyphilic molecules in solution. We shall see below that these tricontinuous patterns emerge naturally from a geometric analysis. We explore in particular the most likely tricontinuous patterns to emerge.

In practice, we model these surfaces using a numerical surface calculation tool called Surface Evolver, which (among other possibilities) determines interfacial geometries from an initial surface approximation *via* minimisation of the total area.²⁹ This geometry tool, available as freeware,³⁰ has proven to be a fruitful method to generate, for example, interfacial geometries for foams³¹ and minimal surfaces.³² Our tricontinuous patterns are built up from patches of minimal surfaces (with zero mean curvature), whose geometries are calculated in Evolver. In addition, a novel ‘modulated honeycomb’ pattern is generated with the help of Evolver, *via* patches of constant (but nonzero) mean curvature.

2 A steric model for polyphile self-assembly: molecular shape vs. triple-line geometry

It is readily proven that self-assembly of three-arm polyphiles must entail at least one infinite connected domain and that the triple-lines are non-intersecting and without ends, *i.e.* they either form closed loops or extend indefinitely.³³ The hexagonal honeycomb is a ‘balanced’ example, with all distinct domains congruent. If we relate the honeycomb geometry to a local polyphile shape, it is clear that the stacking of adjacent molecules along the triple-lines must occur without any torsion, since the interfaces are flat (Fig. 1). It is likely, however, that generic ‘balanced’ polyphiles may exhibit some splay in each arm (assumed here to be equal for all arms in balanced examples). The presence of splay induces a longer triple-line length in the assembly, which can be reduced by a twisted packing between adjacent polyphiles (Fig. 2).

It is therefore feasible that splayed polyphiles prefer to adopt assemblies with nonzero torsion along their triple-lines. Torsion can be introduced in various ways. The simplest pattern that we have built contains alternating right- and left-handed twists of the interfaces along the triple lines of the hexagonal honeycomb, giving a ‘modulated’ triply-periodic hexagonal honeycomb. The walls of this modulated pattern are curved deformations of the flat interfaces of the conventional hexagonal honeycomb. The modulations are introduced by imposing non-zero pressure across the interface, introducing partial bubbles of non-negative and varying Gaussian curvature. We tune the absolute value of the pressure in all three domains to vary the modulations, and build the complete pattern by alternating positive and negative pressure differences in adjacent surface patches to give a pattern with zero net pressure in each domain. The prismatic channels exhibit a cross-section that is generically curved, with oscillating

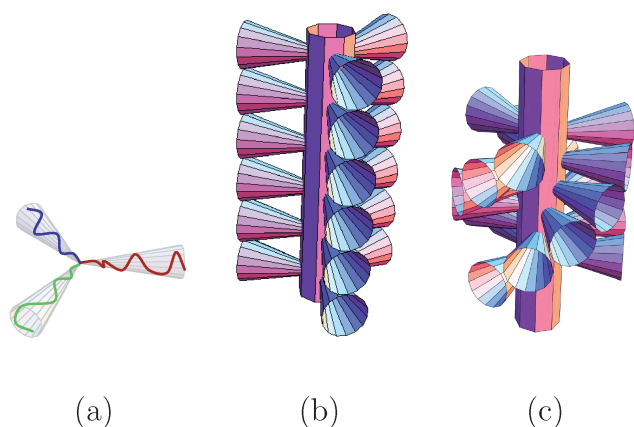


Fig. 2 (a) Schematic cartoon of three-arm polyphile stacking along triple-lines: each arm is represented by a splayed (cone-shaped) block (with empty space between arms for clarity) and a single polyphile is the Y-shaped triplet of arms. (b) Adjacent polyphiles are stacked along the triple-line without twist. (c) Adjacent molecules are twisted along the axis of the triple-line, forcing the interfaces between pairs of arms to adopt a helicoidal form. Twisting allows the molecules to pack with reduced triple-line length, reducing the line tension (at the possible expense of increased surface tension in the interfaces). Adapted from ref. 28.

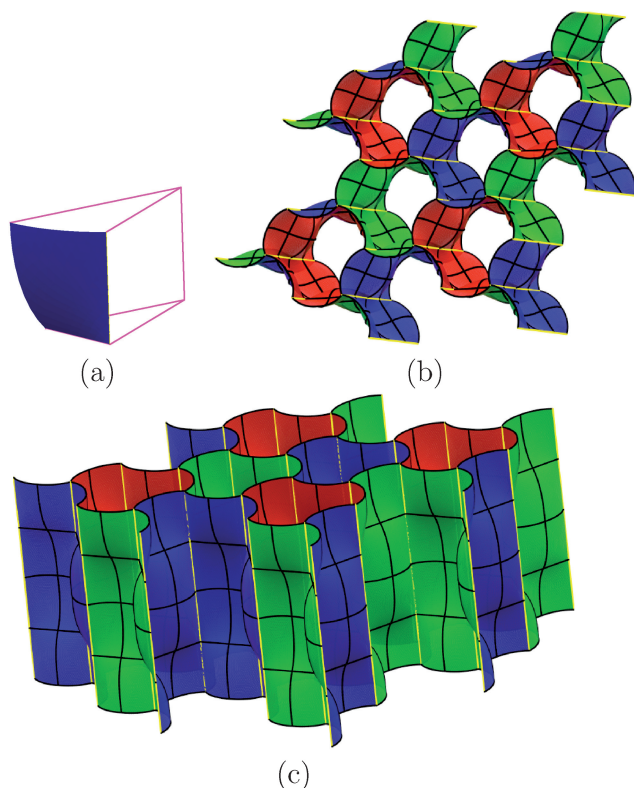


Fig. 3 (a) Surface fragment (of constant, nonzero mean curvature) bounded by straight and curved edges. Repeated reflections in the planes of the curved edges and rotations by π along the straight edges generate a triply-periodic, modulated, hexagonal honeycomb pattern, shown in (b) and (c). This modulated pattern is formed from the simple honeycomb by imposing a periodic twist in alternating right- and left-handed directions along the length of the triple lines (marked in yellow).

convex and concave sections along the triple lines, corresponding to positive and negative pressures, as shown in Fig. 3.

3 Triply-periodic tricontinuous patterns

The imposition of a preferred twist along the triple lines can lead to patterns whose global features differ markedly from the hexagonal honeycomb. Numerous patterns can be built whose interfaces are hyperbolic (non-positive Gaussian curvature) rather than the elliptic or parabolic interfaces found in the modulated and flat hexagonal honeycombs respectively. Hyperbolic interfaces are found in a variety of tricontinuous patterns, that trisect space into a trio of triply-periodic domains. *Tricontinuous* structures (in our sense of the word[†]) are not known to date in soft materials, however, simpler *bicontinuous* analogues are well-known in thermotropic and lyotropic liquid crystals. The latter structures also contain hyperbolic interfaces, that weave through space generating a pair of interwoven domains, rather than the trio of topologically identical labyrinths that characterise our tricontinuous structures. The simplest bicontinuous patterns are formed by triply-periodic minimal surfaces;^{35,36} simple tricontinuous patterns are also built up from minimal surface fragments. The simplest examples of tricontinuous structures trisect space into three geometrically identical labyrinths. We call such structures ‘balanced tricontinuous patterns’.

We use Evolver to determine the geometry of minimal surface patches that span a skew (non-planar) polygonal boundary, analogous to dipping the corresponding skew wire frame in a soap solution to form an open soap film within the frame. In keeping with the terminology of minimal surfaces, we call these surface patches bounded by polygonal circuits *Flächenstücke*. We derive the *Flächenstück* boundary by looking for two- and three-fold rotation symmetry axes that lie in the surface, in the same spirit as that used exhaustively by Fischer and Koch to deduce triply-periodic minimal surfaces, (who determined polygonal boundaries composed of segments of two-fold axes or edges lying in mirror planes).³⁶ Those symmetry operations can be deduced from the pattern of the three-dimensional labyrinth nets that describe the channels of the tricontinuous surfaces. Therefore, as foreshadowed for generic *polycontinuous* patterns,⁴ the construction of tricontinuous patterns can be reduced to one of finding suitable triple intergrowths of triply-periodic nets. This topic is discussed in detail below.

3.1 Names of tricontinuous patterns

A simple naming scheme for balanced tricontinuous structures is desirable. Rather than choose arbitrary names, we describe these patterns using a two-part label *via* their three equivalent interwoven labyrinth nets, based on standard naming schemes for those nets and symmetries. This schema is practical and concise, since it is unlikely that we will encounter distinct tricontinuous

[†] We note that the term ‘tricontinuous’ has been used elsewhere to describe liquid-crystalline structures that are formed by a pair of disjoint hyperbolic interfaces, generating a trio of labyrinths.³⁴ We prefer to reserve the term for a single contiguous, albeit branched surface, that partitions space into three interwoven labyrinths, unlike the mesophase described in ref. 34.

patterns with both the same channel systems and 3D symmetry groups.‡ We name the tricontinuous patterns $3xxx(N)$, where xxx refers to the three-letter code classifying their labyrinth graphs, listed in the on-line database of chemical nets³⁷ and N is the space group number of the pattern displaying three symmetrically distinct labyrinths, corresponding to the three-coloured pattern. (Within this nomenclature system, the P , D and G (yroid) bicontinuous patterns adopt the names $2pcu(221)$, $2dia(227)$ and $2srs(214)$, respectively.)

3.2 Balanced tricontinuous patterns defined by linear *Flächenstücke* containing three-fold axes

Our strategy for detecting promising balanced tricontinuous candidates is motivated by Alan Schoen's approach to deducing triply-periodic minimal surfaces (that give bicontinuous spatial patterns): among the infinite number of possible patterns, he focused primarily on those that can be built from smallest *Flächenstück* boundary polygons composed of straight lines. This strategy is a very effective one for targeting the patterns seen in bicontinuous mesophases of soft materials. For example, within the infinite variety of bicontinuous patterns derived from triply-periodic minimal surfaces, only the P and D triply-periodic minimal surfaces (giving, en route, the *gyroid* pattern also) are generated from skew quadrilateral boundary polygons; all others are built from pentagons, hexagons, and higher polygons (or more complex boundaries). It is noteworthy that the P , D and *gyroid* surfaces are precisely those most commonly found in bicontinuous mesophases of soft materials,³⁵ likely due to the relatively homogeneous local and global geometries induced by small polygons.³⁸ We note also that it is likely that among all triply-periodic minimal surfaces, those with the lowest possible genus per unit cell – three – furnish the most homogeneous candidates³⁹ and these simplest minimal surfaces are related to so-called 'minimal nets'.⁴⁰ These observations have guided our search for suitable tricontinuous patterns that are realisable in soft materials.

We have explored, in some detail, triple intergrowths of relatively simple nets, as a route to constructing the simplest (and therefore likely the most favoured) tricontinuous patterns. In particular, we have looked at triple intergrowths of minimal (genus – three per unit cell) nets, that yield low-genus labyrinths in tricontinuous patterns. A variety of intergrowth modes are possible, each combining different combinations of nets. We note that distinct nets may yield the same tricontinuous pattern. We therefore determine the three *labyrinth graphs* of the tricontinuous pattern formed by branched minimal surfaces – one for each channel system – which describe the axes of the channel pattern and compare it with the pattern formed by the initial trio of interpenetrating nets. The resulting labyrinth graphs are calculated numerically by a process of homotopic thinning, that ensures the graphs respect the initial topology of the channel systems using a medial axis algorithm contained within the Mango software package.⁴¹ In some cases, the labyrinth graphs coincide with the starting nets, in other cases they differ. A fuller

analysis is beyond the scope of this paper and will be published elsewhere.

Simplest tricontinuous surfaces may contain a minimal-surface *Flächenstück* bounded by straight lines which lie in two- and three-fold rotational axes, from which the entire pattern can be generated by repeated rotations. Among these cases, we select those whose triple lines extend indefinitely throughout space under the action of the symmetry elements without inducing vertices along the lines. In other words, all branch lines are non-intersecting, in keeping with the constraint on polyphilic assemblies discussed at the beginning of section 2. Those *Flächenstücke* are related to global symmetries of the trio of nets that are used to determine the channels of the tricontinuous pattern via the following prescriptions. Three-fold rotation axes that exchange the nets ($A \rightarrow B$, $B \rightarrow C$ and $C \rightarrow A$) necessarily give straight three-fold branch-lines in the surface. Similarly, two-fold axes that swap pairs of nets (and are isometries of the third net) give straight lines in the related minimal surface. These polygonal circuits are used to build Evolver input files, and the resulting output is a minimal-surface *Flächenstück* bounded by the polygon. The complete tricontinuous pattern is formed by repeated rotations of the *Flächenstück* about its two- and three-fold bounding edges.

An example of this procedure is the tricontinuous pattern that emerges from rhombohedral intergrowths of triply-cubic

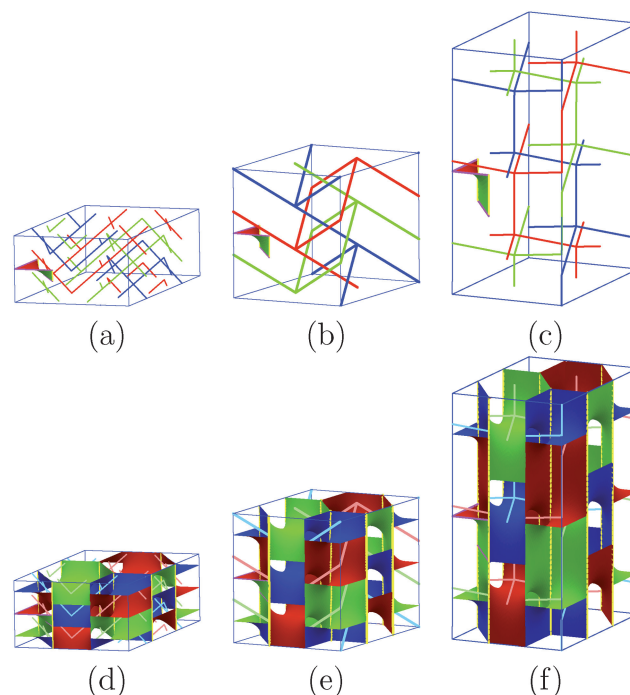


Fig. 4 Tricontinuous, trigonal, open cellular structures built from polygonal *Flächenstücke* bounded by two- and three-fold rotational symmetry axes of patterns composed of three interwoven (left to right) *nbo*, *dia* and *pcu* nets. (a–c) show the nets with a single *Flächenstück*, (d–f) fragments of the complete triply-periodic patterns: (d) $3nbo(160)$, (e) $3pcu(160)$ and (f) $3dia(160)$. Note that these three patterns are members of a one-parameter family of structures related by a uniaxial stretch parallel to the three-fold axis (marked by yellow lines). A magnified view of the $3pcu(160)$ pattern is shown in Fig. 5.

‡ The converse, however, is not true. We shall see below a number of triple intergrowths of distinct nets that lead to tricontinuous surfaces that are essentially the same, and differ only in that they are uniaxial distortions of each other. Therefore a single polycontinuous surface family may be characterised by a number of different nets.

diamond (dia^{37}) nets, $3dia(160)$ and the related intergrowth of three primitive cubic (pcu^{37}) nets, $3pcu(160)$ and three tetragonal nbo nets,³⁷ $3nbo(160)$, shown in Fig. 4. These nets contain intersecting two- and three-fold rotation axes, leading to simple *Flächenstücke* bounded by skew pentagons with vertex angles of $\frac{\pi}{2}, \frac{\pi}{2}, \frac{\pi}{2}, \frac{\pi}{2}, \frac{\pi}{3}$. The polygons differ only in the length of their pair of parallel edges; with respect to the rhombohedral unit cell edges **a** and **c**, the $\frac{c}{a}$ ratios for $nbo:pcu:dia$ are 1 : 2 : 4 respectively.

Flächenstücke for these net intergrowths, shown in Fig. 4, are therefore also similar. The tricontinuous patterns are shown in Fig. 4. The labyrinth graphs of these three surfaces are the same as the starting nets for the $3dia(160)$ and $3pcu(160)$ cases. In contrast, the $3nbo(160)$ cellular pattern relaxes in Evolver to give a surface whose labyrinth graphs (calculated by Mango) are equivalent to a pcu net, albeit compressed along a single three-fold axis (parallel to the rhombohedral **c**-axis). We therefore collapse these three examples into a single one-parameter family of tricontinuous surfaces, whose members are characterised by the value of their $\frac{c}{a}$ ratio.

In stark contrast to the triply-periodic minimal surfaces, no examples of skew quadrilaterals with unbranched or non-intersecting three-fold lines have been found. We have found just three examples of tricontinuous patterns made of branched minimal surfaces that can be constructed by repeated rotations around the linear boundary edges of skew pentagons and hexagons. These cases are described in more detail in the next sections.

3.2.1 Tricontinuous, trigonal *P* and *D* analogues: $3dia \dots pcu(160)$. The smallest *Flächenstück* giving tricontinuous surfaces containing infinite, vertex-free three-fold lines are skew linear pentagons, with vertex angles of $\frac{\pi}{2}, \frac{\pi}{2}, \frac{\pi}{2}, \frac{\pi}{2}, \frac{\pi}{3}$, found in the examples described above. The labyrinth graphs of this one-parameter family of patterns vary with the axial ratio of the rhombohedral lattice (a parameter that depends on the height of the trigonal prism bounding the pentagonal *Flächenstück*, whose

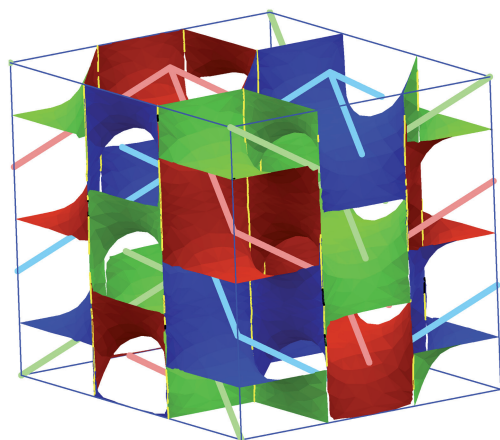


Fig. 5 (a) $3pcu(160)$: The open cellular pattern with trigonal symmetry that trisects space into three interpenetrating labyrinths formed by inflating three pcu nets (cf. Fig. 4).

angles can be conserved within a one-parameter family of deformations).

For certain values of that parameter, the resulting tricontinuous surface exhibits labyrinth graphs that correspond to $3pcu(160)$ (illustrated in Fig. 5) and $3dia(160)$ nets. For axial $\left(\frac{c}{a}\right)$ ratios larger than *ca.* 2 the three labyrinth graphs determined by Mango are trigonal distortions of *dia* nets; for smaller values of axial ratios, distorted *pcu* nets result.

The cubic $3dia(160)$ and related structures are (branched) minimal-surface trisections of space, analogous to the *D* ($2dia$) and *P* ($2pcu$) surfaces, that bisect space, forming equivalent labyrinth graphs.

3.2.2 Tricontinuous hexagonal structures: $3etc(187)$. Skew hexagons, with vertex angles of $\frac{\pi}{3}, \frac{\pi}{2}, \frac{\pi}{2}, \frac{\pi}{2}, \frac{\pi}{3}$, are found in the hexagonal (one-parameter family of) branched surfaces described by *etc*³⁷ labyrinth graphs (Wells' (8, 3) – *c*) nets⁴²), denoted $3etc(187)$ and illustrated in Fig. 6. This structure shares the set of three-fold branch lines of the hexagonal honeycomb; in contrast to the latter, $3etc(187)$ contains hyperbolic (minimal-surface) walls and 'three-dimensional domains' (connected labyrinths extending to infinity in all directions.)

3.2.3 A tricontinuous orthorhombic gyroid analogue: the $3srs(24)$ pattern. A branched orthorhombic structure, $3srs(24)$, whose labyrinths are described by cubic *srs* nets³⁷ (Wells' (10, 3) – *c* net,⁴²) also contains a skew hexagon with vertex angles $\frac{\pi}{2}, \frac{\pi}{2}, \frac{\pi}{2}, \frac{\pi}{2}, \frac{\pi}{2}, \frac{\pi}{2}$ (Fig. 7). This surface is very close to a global

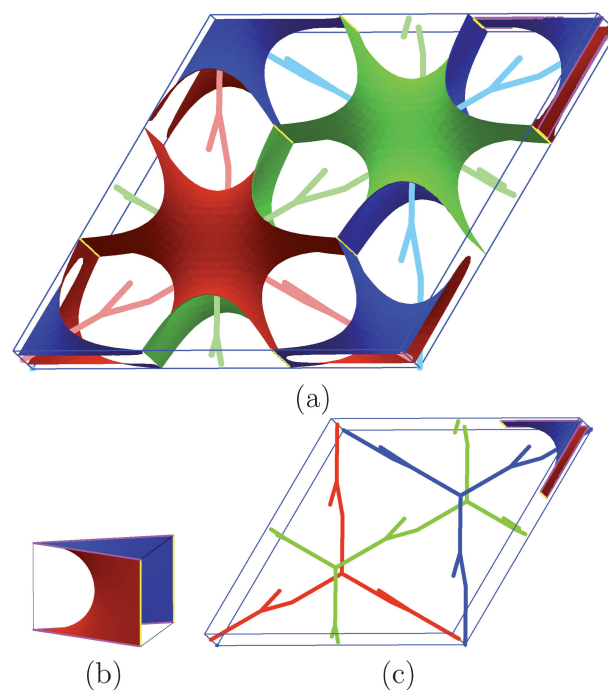


Fig. 6 (a) $3etc(187)$: An open cellular pattern with hexagonal symmetry that trisects space into three interpenetrating *etc* nets. (b) The minimal-surface *Flächenstück*. (Vertical (yellow) edges denote the pair of three-fold lines). (c) Corresponding three-fold interpenetration of *etc* nets.

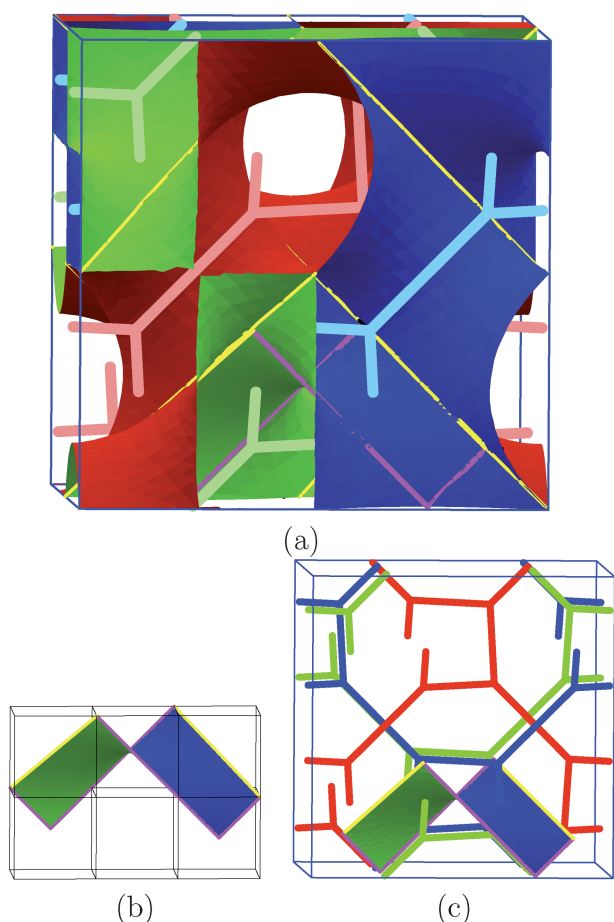


Fig. 7 $3srs(24)$: (a) An open cellular tricontinuous pattern, which exhibits orthorhombic symmetry, and trisects space into three interpenetrating *srs* nets. Each domain is described by a like-handed *srs* net. (b) Minimal-surface *Flächenstück*. (c) Corresponding three-fold interpenetration of *srs* nets with a single *Flächenstück* in place.

extension of the local branched ‘Archimedean screw’ structure analysed by Elser in 1996; Elser’s example gives a geometrically similar structure with slightly variable mean curvature, in contrast to our zero-mean-curvature case.⁴³ The $3srs(24)$ structure is analogous to the *gyroid*, which bisects space into an enantiomeric pair of *srs* labyrinths – in contrast to $3srs$, which contains a trio of like-handed *srs* labyrinths.

3.3 Balanced tricontinuous patterns with *Flächenstücke* free of three-fold axes

The previous examples were all constructed by repeated two- and three-fold rotations around the linear edges making up the *Flächenstück* boundary. They can also be built without the imposition of skeletal in-surface lines induced by the rotational symmetry constraints, by assuming only triply-periodic translational symmetry, as follows. The polycontinuous pattern is assumed to contain a trio of mutually interpenetrating labyrinths, defined by the seed nets, *e.g.* $3etc(187)$, shown in Fig. 8(a). First, we build a cellular pattern equivalent to the Voronoi domains around each vertex of a single unit cell of the three nets (red, green and blue), and impose periodic boundary conditions. (In some cases, to form a more faceted ‘seed structure’, we add

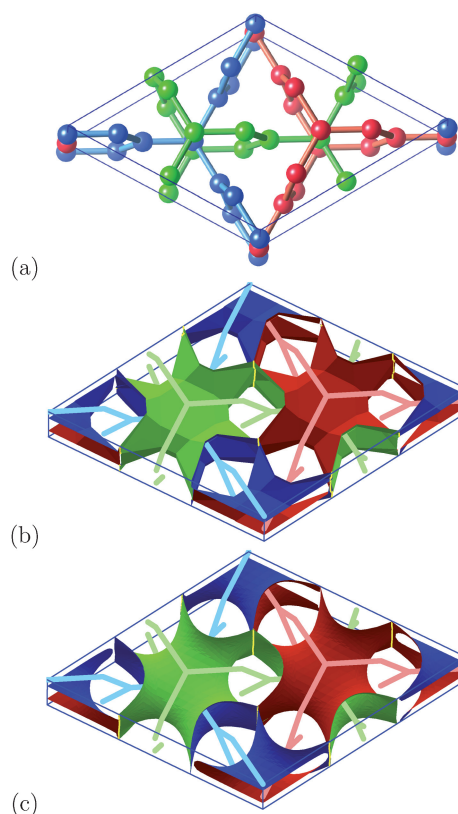


Fig. 8 Constructing a tricontinuous pattern. (a) Starting pattern of three interwoven $3etc(187)$ nets. (b) Voronoi cellular decomposition of the vertices of the *etc* nets in (a), excluding all faces that separate vertices of the same colour. (c) Annealed $3etc(187)$ tricontinuous pattern formed by relaxing the interfaces in (b) using Evolver, assuming equal volumes in all three labyrinths and imposing periodic boundary conditions.

extra vertices on the net mid-edges.) To form a tricontinuous structure, we require infinite labyrinths that are threaded by the nets. We therefore discard all faces of the Voronoi domain that are intersected by edges of the nets; *i.e.* faces that separate vertices of the same colour in adjacent cells (Fig. 8(b)). Finally, we relax the remaining facets that separate unlike-coloured vertices with the aid of Evolver, giving walls of zero mean curvature and locally minimal area subject to the constraint of equal volumes in all three labyrinths (Fig. 8(c)).

This approach generates identical patterns to those formed by extending the polygonal *Flächenstück* throughout space by two- and three-fold rotations for the three tricontinuous patterns discussed in section 3.2. However, we have found many other examples of triple intergrowths of simple nets whose symmetries do not admit skeletal frameworks of two- and three-fold rotation axes. In these cases then, we can form neither a simple linear polygonal boundary nor a *Flächenstück*. However, since these patterns also display translational symmetry, we can use the Voronoi domain to form seed patterns, from which Evolver can deduce a relaxed pattern consisting of minimal, (or near-minimal) surface patches. We then search for an approximate *Flächenstück*, bounded by straight lines, that we can use to model relative energies of the related balanced tricontinuous pattern within the relaxed tricontinuous pattern. In the cases discussed below, these *Flächenstücke* are formed by straightening helical triple lines, and

the approximation is a good one for helices of long pitch. Note that the symmetry operations along these triple lines need no longer be three-fold rotations, as was the case for the previous examples. We find examples here where the *Flächenstücke* are extended across their triple-lines by a euclidean screw operation. This approach yields data for three additional balanced tri-continuous families, approximated by pentagonal *Flächenstücke* and allows extension of the $3srs(24)$ pattern to a one-parameter family of patterns, approximated by a hexagonal *Flächenstück*.

3.3.1 Tricontinuous triclinic gyroid family: the $3srs(1)$ pattern.

The $3srs(24)$ pattern is orthorhombic, despite each isolated *srs* labyrinth displaying cubic symmetry. It can therefore be distorted in a variety of ways within the orthorhombic setting. Among those possibilities, we choose the deformation mode that retains a single set of parallel, straight, triple lines (and leads to helical triple lines in other directions). This is readily done within the ‘uncoloured’ structure, for which all $3srs$ nets are considered to be symmetrically equivalent. We can embed the uncoloured nets into a rhombohedral setting, allowing a one-parameter family of structures, distinguished by their repeat distance along the three-fold axis ($\frac{c}{a}$ ratio). We call this one-parameter family of (coloured) triclinic patterns $3srs(1)$. Generic members of this family contain distorted channels, with trigonal rather than the cubic symmetry

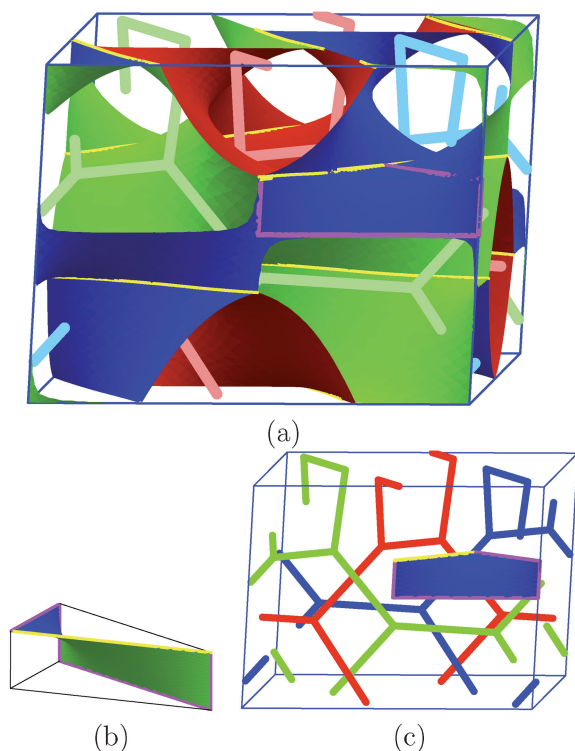


Fig. 9 (a) $3eta(145)$: An open cellular pattern with trigonal symmetry that trisects space. This particular example is the member of a one-parameter family of surfaces that trisects space into three interpenetrating *eta* nets or three distorted *qtz* nets (cf. Fig. 10). The approximate polygonal *Flächenstück* is overlaid in the figure, bounded by three-fold (yellow) and two-fold (purple) straight edges. (b) Approximate minimal-surface *Flächenstück*. (c) Corresponding three-fold interpenetration of *eta* nets.

of the regular *srs* net. We form a *Flächenstück* in these patterns corresponding to the linear hexagonal *Flächenstück* found in the single orthorhombic $3srs(24)$ example. This polygonal *Flächenstück* approximates a patch of the tricontinuous $3srs(1)$ surface to varying degrees, depending on the axial ratio of the pattern; generic $3srs(1)$ patterns give a surface patch that is not bounded by straight lines, rather they are slightly curved.

3.3.2 Trigonal patterns: $3qtz(145)$. Triple intergrowths of many hexagonal nets can be formed that result in elegant patterns. Among the many examples that we have explored, an additional one-parameter family of rhombohedral balanced tri-continuous patterns emerges that is well approximated by a skew linear pentagon. The complete pattern is formed by extending the *Flächenstück* across its bounding edges *via* two-fold rotations along the unbranched lines and a screw operation (composed of a rotation and a translation along the line) along the three-fold lines. The operation is of type 2_1 with reference to the crystallographic cell of the uncoloured structure (that allows symmetry operations exchanging channels).

The related one-parameter family of trigonal patterns include partitions formed by triply-interwoven *eta* (Wells’ (8, 3) – *a*) nets⁴² and *qtz* (quartz,³⁷) nets. Analysis of the $3eta$ pattern shows that the labyrinths determined by Mango are distorted *qtz* nets (degree-four) rather than *eta* nets. We therefore call this the $3qtz(145)$ family. These two specific members of the family, with regular *eta* and *qtz* nets (³⁷) are illustrated in Figs. 9,10.

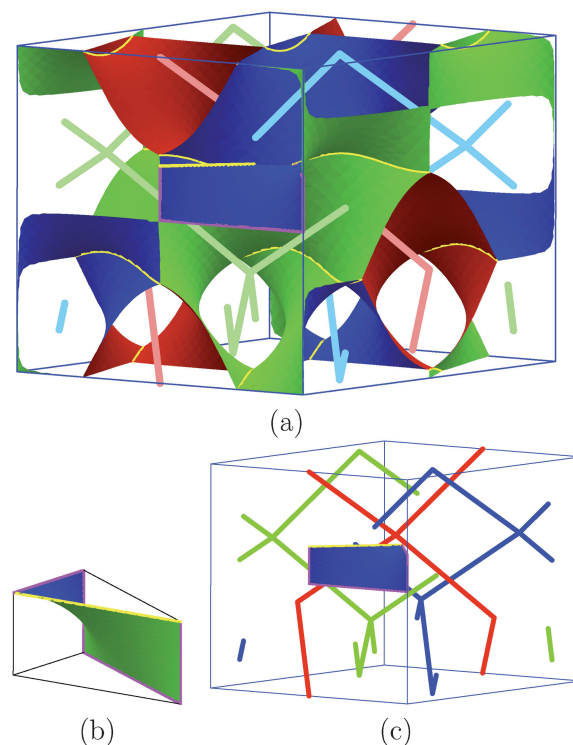


Fig. 10 (a) $3qtz(145)$: An open cellular pattern with trigonal symmetry that trisects space into three interpenetrating *qtz* nets, showing the three-fold (yellow) extended branch lines. The approximate polygonal *Flächenstück* is overlaid in the figure, bounded by three-fold (yellow) and two-fold (purple) straight edges. (b) Approximate minimal-surface *Flächenstück*. (c) Corresponding three-fold interpenetration of *qtz* nets.

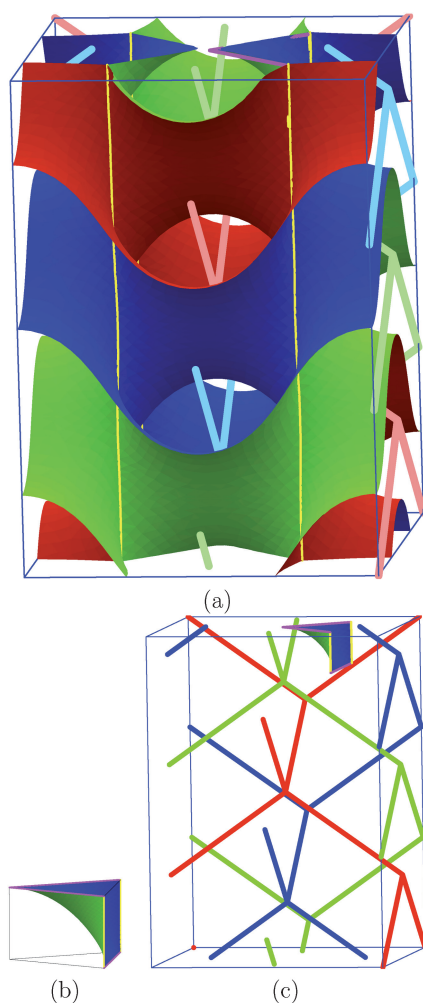


Fig. 11 (a) *3dia*(109): An open cellular pattern with tetragonal symmetry that trisects space into three interpenetrating *dia* nets. (b) Approximate minimal surface *Flächenstück* bounded by a screw-axis (yellow) along the triple line and two-fold (purple) straight edges. (c) Corresponding three-fold interpenetration of *dia* nets.

3.3.3 Tetragonal diamond patterns: *3dia*(109). Lastly, a very uniform 3D weaving of *3dia* graphs – distinct from that in the trigonal *3dia*(160) case – gives a branched tetragonal *3dia*(109) surface with three threaded (cubic) *dia* labyrinth graphs, shown in Fig. 11. The zero-mean-curvature version of this surface, realised by Evolver, contains parallel triple-lines that are helical with a large pitch-to-radius ratio; we choose an approximate *Flächenstück* boundary that models those helices as straight lines, giving another skew pentagonal boundary with vertex angles $\frac{\pi}{2}, \frac{\pi}{2}, \frac{\pi}{2}, \frac{\pi}{2}, \frac{\pi}{4}$. The complete pattern is generated by extending across the three-fold lines by a screw operation (a 4_1 operation with respect to the unit cell of the uncoloured pattern). Stretching or compressing this structure along the triple line deforms the labyrinths away from their most symmetric (cubic) *dia* net geometry, and generates a one-parameter family of related patterns of tetragonal symmetry.

4 Structural chirality

The presence of torsion in these structures theoretically admits the possibility of spontaneous chirality in related self-assembled

systems. Among the patterns introduced here, the *3qtz*(145) family, as well as the *3srs*(24) families adopt chiral symmetries for the 3D patterns, assuming all three domains are symmetrically distinct. In contrast, the *3dia*·*pcu*(160), *3etc*(187) and *dia*(109) families are achiral. Note that the global chirality is independent of the torsion along the three-fold branch lines: the *3srs*(24) structure contains alternating clockwise–anticlockwise twist along the lines, while the *3qtz*(145) family exhibits line torsion in one sense only along all three-fold branch lines.

5 Tricontinuous energies and interfacial geometry

We build a first-order ‘steric’ model for these structures, with equal volumes in all domains and equal surface tensions at all interfaces, which assumes only a preferred twist. This parameter is set by the molecular splay at the junctions; any tricontinuous structure (with equal domain volumes) can be tuned by selection of the lattice scaling to adopt the preferred twist.

We can compare self-energies for various structures in a number of ways. The most significant energetic contribution is the surface area per volume (scaled per unit triple line-length; that itself scales with volume per molecule, or solvent/molecule composition). Suppose the evolved pattern has area Σ_0 and triple-line length λ_0 per unit cell of volume V_0 (trisected into three equal volumes). The area (Σ) per volume (V) scales with the homothetic scale factor of the underlying lattice, c , as $\frac{\Sigma}{V} = \frac{\Sigma_0}{V_0} c^{-1}$. The triple-line length (λ) per volume scaling is $\frac{\lambda}{V} = \frac{\lambda_0}{V_0} c^{-2}$, so that the energy, E_s is given by:

$$E_s = \sigma \frac{\Sigma}{V} = \sigma \frac{\Sigma_0}{V_0} \left(\frac{\lambda}{V} \frac{V_0}{\lambda_0} \right)^{\frac{1}{2}} \quad (1)$$

where σ is the surface tension, assumed for convenience here to have the same value for all three interface types (AB, BC and CA). It is convenient to introduce the dimensionless parameter $\varepsilon := \frac{V\lambda}{A^2}$, defined originally by Elser to characterise the scale-free length-to-area ratio of his branched surface.⁴³ The model energy can then be written:

$$E_s = \sigma \varepsilon^{-\frac{1}{2}} \left(\frac{\lambda}{V} \right)^{\frac{1}{2}} \quad (2)$$

where the value of $\frac{\lambda}{V}$ depends on the molecular stacking, set by the distance between molecular junctions λ , and V is the total volume per polyphile molecule (plus associated solvents, where applicable). Within this approximation, it follows that the relative energies between distinct spatial trisections depend only on $\varepsilon^{-1/2}$. Distinct structures, however, will embody different torsions along the triple-line.

At this point, we may choose to impose an energy cost depending on the difference between the structural torsion and the most favoured torsion per molecule, again set by the atomic details of the polyphile architecture. This route is comparable to the bending energy formalism of molecular membranes, which gives an elastic energy cost, depending on the deviations of

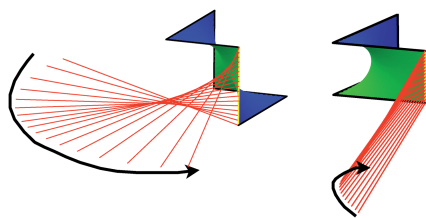


Fig. 12 The curvature of the *Flächenstück* within these tricontinuous structures induces torsion along the three-fold branch lines, allowing adjacent polyphiles to pack with a mutual twist. The figure shows (left) the torsion along a *3pcu*(160) *Flächenstück* and (right) along a *3etc*(145) *Flächenstück*.

membrane curvatures away from their ‘preferred’ or relaxed values.⁴⁴ For simplicity, we first assume a rigid packing model, with no deviations from a preset torsion. We therefore determine relative energies for various structures *via* their $\varepsilon^{-1/2}$ values, paired with the torsion of the pattern, scaled by the homothetic factor, c , which allows the pattern to adopt the desired value of $\frac{\lambda}{V}$ (for convenience here, assumed to be unity.)

The torsion along these triple-lines experienced by arms of the polyphile is equal to the variation of surface normal vector (\mathbf{n}) with arc-length along the lines. This torsion depends on the curvature of the surface *Flächenstück* along the triple-line, as illustrated in Fig. 12.

The torsion can also be related explicitly to the curvature of the minimal-surface elements making up the tricontinuous patterns as follows. The Bonnet–Kovalevsky formulae of differential geometry relate the variation of surface normal vector with arc-length ($\dot{\mathbf{n}}$) to the tangent vector to the (triple-)line (\mathbf{t}), the binormal vector along the line (\mathbf{b}), the geodesic torsion (τ_g) and the normal curvature (k_n) along the (triple-)line:⁴⁵

$$\dot{\mathbf{n}} = -k_n \mathbf{t} - \tau_g \mathbf{b}$$

In our case, the normal curvature vanishes, by our assumption of uncurved triple-lines. The torsion along these lines is therefore equal to the geodesic torsion of the asymptotes on the surface, which is dependent only on the principal curvatures of the surface (k_1 and k_2) and the angle with principal directions, ϕ :⁴⁶

$$\tau_g = \frac{1}{2}(k_1 - k_2) \sin 2\phi \quad (3)$$

Generic patterns contain triple lines subtending arbitrary angles with the principal directions of the three surface elements that meet along the line. However, these balanced tricontinuous patterns have triple-lines that we assume here are curvature-free for all cases and interfaces that are minimal surfaces, characterised by the relation $k_1 + k_2 = 0$. It follows that the straight triple-lines lie along the asymptotic directions of the minimal surfaces, rotated by an angle ϕ of $\frac{\pi}{4}$ from the principal directions. In these cases the torsion is simply related to the Gaussian curvature $K(p)$ of the surface element at each point p on the triple-line:

$$\tau_g(p) = \sqrt{-K(p)} \quad (4)$$

(This result holds in fact for any hyperbolic surface whose triple-lines are straight.)

As a first approximation, we assume negligible variations of curvature homogeneity over the interface, similar to the homogeneity approximation employed to estimate preferred bicontinuous structures in amphiphilic molecular bilayer assemblies.⁴⁷ Within this homogeneous curvature approximation, we can estimate the Gaussian curvature from

$$K(p) \approx \langle K \rangle = \frac{\iint K(p') dA}{A} \quad (5)$$

The numerator of this expression can be calculated exactly from the local Gauss–Bonnet formula for a surface bounded by a geodesic n -sided polygon, with interior vertex angles, θ_i :

$$\iint K(p') dA = (2 - n)\pi + \sum_{i=1}^n \theta_i \quad (6)$$

This relation between torsion and Gaussian curvature allows us to estimate a ‘smeared’ torsion value, including contributions of the torsion away from the triple-lines, discussed in the next section.

6 Relative energies of crystalline tricontinuous patterns

We have estimated the relation between the energy of various patterns, calculated using eqn (2), and the torsion experienced by neighbouring molecules stacked along the branch-lines for all five surface families: *3dia*·*pcu*(160), *3etc*(187), *3srs*(24), *3qtz*(145) and *3dia*(109). Note that we assume (without loss of generality within our balanced model) unit surface tension and unit triple-line length per volume. We estimate the torsion using two distinct approximations, described below.

We first assume that the molecular junctions occupy negligibly small area and are confined exactly to the straight three-fold branch lines, so that the torsion values calculated on the triple-lines are accurate measures of the twist between adjacent molecules. Within this local approximation, we need only estimate the torsion along the triple-lines, which can be calculated directly from the angle between consecutive surface normals (Fig. 12). This information has been extracted directly from the Evolver data files. The results are plotted in Fig. 13(a).

At the other extreme, the junctions can be assumed to be smeared over the surfaces, rather than being confined to the lines. The real situation is likely to lie somewhere between complete delocalisation of torsion and idealised localisation to the triple-lines alone, depending on the size and stacking of adjacent star polyphile junctions. The assumption of perfect curvature homogeneity over the surfaces, introduced in eqn (5), though imperfect, allows us to estimate the torsion within this approximation, *via* averaging over a complete asymmetric element (*Flächenstück*) of the tricontinuous pattern. Note from eqn (3) that an upper bound on the (magnitude of the) torsion is realised

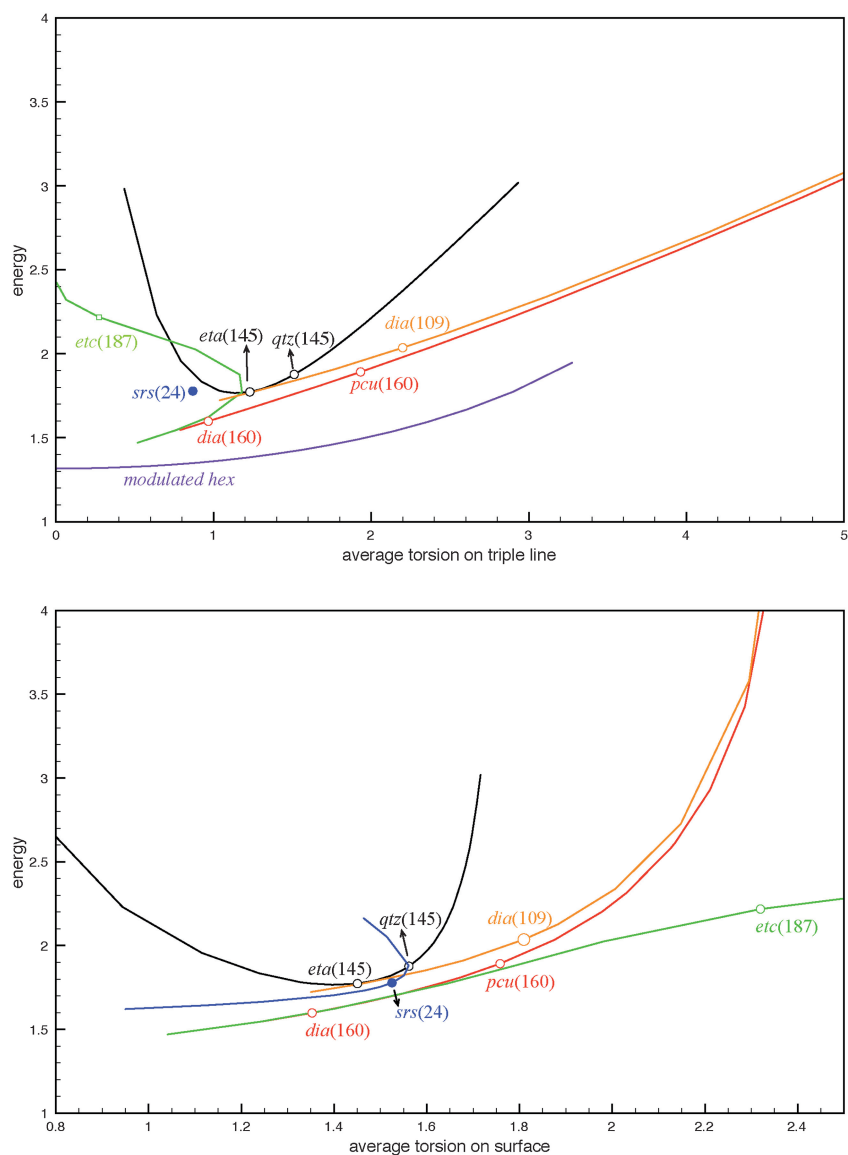


Fig. 13 Plots of relative energies of balanced tricontinuous partitions vs. torsion. (a) The torsion is determined by averaging its value over the entire surface. (b) The torsion is an average value along the triple-line.

when $\phi = \pi/4$, when the triple-lines are aligned with the asymptotic directions in the minimal surface. That is necessarily the case when the triple-lines are straight. However, assuming delocalisation of the junctions, the vectors joining adjacent molecular junctions need not lie along asymptotic directions. Nevertheless, regardless of their orientation, the torsion magnitude cannot exceed the value that follows assuming $\phi = \pi/4$. We use the vertex angles of the polygonal (geodesic) boundaries of the Flächenstück to calculate the integral Gaussian curvature, *via* eqn (6), from which the area-average value of the Gaussian curvature can be estimated, which leads to the upper bound on the torsion *via* eqn (4). Those values are then paired with relative energies calculated from eqn (2). These data are collected in Fig. 13(b).

We note first that for very low values of the preferred torsion, corresponding to polyphile molecular architectures with little splay of their arms from the central junction outwards,

tricontinuous structures are unlikely, since the hexagonal honeycomb partition (Fig. 1), with vanishing torsion along the triple-lines (and $\varepsilon^{-1/2} = 3^{1/4} \approx 1.32$) give lower interfacial areas. Indeed, neglecting for the moment the energy cost due to variations of torsion, the modulated hexagonal honeycomb (Fig. 3) is favoured over tricontinuous structures. Among the latter class of structures, relative energies of distinct surface families diverge significantly.

In the low torsion regime, stretched versions of the $3etc(187)$ structure and the $3dia(160)$ member of the $3dia \cdot pcu(160)$ family of patterns are the most favourable tricontinuous morphologies for both models, though less so than the modulated hexagonal pattern. For intermediate torsion values, all tricontinuous structures have comparable energies.

The situation is more complex for highly splayed systems, that impose high values of the spontaneous torsion. Within the approximation that assumes all molecular junctions are located

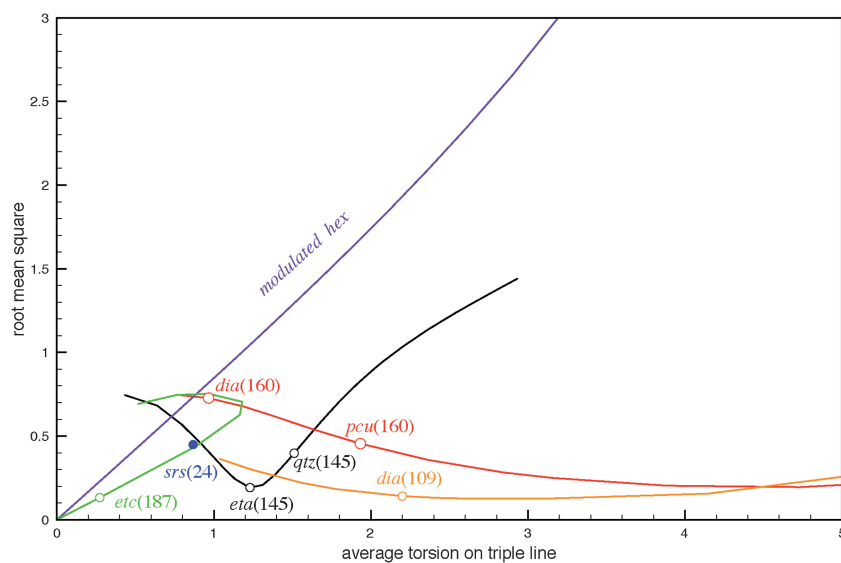


Fig. 14 Estimates of the root-mean-square torsion along the triple-lines, plotted against the average torsion, indicative of the inhomogeneity of torsion along the triple-lines.

precisely on the triple-lines, members of the $3dia(109)$ family (with low $\frac{c}{a}$ ratios) compete with stretched $3pcu(160)$ members of the $3dia \cdot pcu(160)$ family for the lowest relative energies. On the other hand, if we assume delocalisation, the situation is less clear, since then we have only upper bounds on the torsion. However, assuming those bounds are not too loose, ‘squashed’ versions of the $3etc(187)$ structure (with small $\frac{c}{a}$ ratios) are most favoured.

7 Inhomogeneous torsion: beyond the steric model

So far, we have considered averages, either throughout the surface *Flächenstück* or along the triple-lines. In fact, these surfaces are necessarily inhomogeneous, with varying Gaussian curvature. Assuming a strictly preferred value of the spontaneous torsion, those variations are expected to induce an additional energy cost, in addition to the surface energy due to the interfaces. The torsion inhomogeneities along the triple-lines have been estimated numerically using Evolver, from which data we have calculated the second moment of the torsion along the line, *via* the root-mean-square value. These data are plotted in Fig. 14. We may think of this cost as the analogue of the elastic bending energy incurred by amphiphilic bilayers with a spontaneous curvature. Such inhomogeneities allow us to go slightly beyond the simple steric model, used so far. However in the absence of details of the relative magnitudes of moduli of surface area (surface tensions) and torsion, we cannot sum area and torsional variations to deduce a conclusive structural hierarchy. Nevertheless, we can and will draw some conclusions from these additional data.

Here too, three regimes are apparent, corresponding to the low-, intermediate-, and high-torsion regimes introduced in the previous section. The data reveal substantial differences in inhomogeneity of the torsion between the modulated hexagonal honeycomb and the tricontinuous examples. Indeed, if a strictly preferred value of the torsion is required, the modulated

hexagonal pattern is disfavoured beyond very small values of the spontaneous torsion. Within the low-torsion regime, stretched versions of the $3etc(187)$ structure are most favoured. At intermediate values, $3qtz(145)$ morphologies are marginally favoured over the $3dia(160)$ structures, assuming the approximation of straight triple-lines used here (an approximation that imposes some uncertainty on these two structural classes.)

The inhomogeneity contributions further substantiate the earlier conclusion that highly splayed systems – imposing high torsion values – are likely to adopt squashed $3pcu(160)$ or $3dia(109)$ tricontinuous structures.

8 Conclusions

We expect an interesting structural polymorphism within polyphile self-assemblies. The tricontinuous $3dia(160)$ and/or $3etc(187)$ structures are expected to be the most favourable tricontinuous structures for low values of the spontaneous torsion, in competition with a novel modulated hexagonal honeycomb pattern. For intermediate torsion, all tricontinuous structures considered here are of comparable energy, and are favoured over the modulated hexagonal structure if variations about the preferred value of the torsion are energetically costly. Finally, for large values of the spontaneous torsion, squashed $3pcu(160)$ patterns as well as squashed members of the $3dia(109)$ family are favoured, along with squashed members of the $3etc(187)$ family.

A useful rule of thumb for ranking bicontinuous patterns is the following. The most favourable patterns have asymmetric surface domains of minimal (absolute) Gaussian integral curvature. Ordered bicontinuous patterns are overwhelmingly dominated by patterns derived from the family of triply-periodic minimal surfaces related to the *P*, *D* and *gyroid* structures (with labyrinth graphs $2pcu$, $2dia$ and $2srs$ respectively). Among all triply-periodic minimal surfaces, these examples have the ‘smallest’ asymmetric 2D hyperbolic domains (characterised by the area of the related orbifolds, see⁴⁸), bounded by triangles with

vertex angles $\frac{\pi}{2}$, $\frac{\pi}{4}$ and $\frac{\pi}{6}$, whose edges correspond to the in-surface reflection lines (forming the *246 hyperbolic orbifold). The corresponding domains for our candidate tricontinuous branched minimal-surface patterns are skew $\frac{\pi}{2}$, $\frac{\pi}{2}$, $\frac{\pi}{2}$, $\frac{\pi}{8}$ in the 3dia(109) family (the *2228 hyperbolic orbifold, with area $\frac{3}{16}$), since the corresponding *Flächenstücke* are bisected by a mirror line. The asymmetric domains of the 3dia...pcu(160) family as well as the 3etc(187) patterns are quadrilaterals with vertex angles $\frac{\pi}{2}$, $\frac{\pi}{2}$, $\frac{\pi}{2}$, $\frac{\pi}{6}$ (forming the *2226 hyperbolic orbifold, with area $\frac{1}{6}$); skew $\frac{\pi}{2}$, $\frac{\pi}{2}$, $\frac{\pi}{2}$, $\frac{\pi}{2}$ pentagons for the qtz(145) family (the *2⁵ hyperbolic orbifold, with area $\frac{1}{4}$). The 3srs(24) asymmetric domain (Fig. 7), bounded by the skew linear hexagon discussed above contains a 2-fold axis normal to the *Flächenstück*, passing through the centre of the polygon, so that the asymmetric domain is a half that of the total polygon, with orbifold symmetry 2*222 (area $\frac{1}{4}$). The surface families can be sorted from smallest to largest orbifold areas, giving the following ranking from most to least homogeneous: 3etc(187), 3dia...pcu(160) > 3dia(109) > 3srs(24) ~ 3qtz(145). It is interesting to notice that this ranking is in rough agreement with that inferred from the steric and elastic models deduced in the previous section.

We point out that we have studied more than a dozen additional candidate structures (characterised by their labyrinth graphs); all of those other candidates have larger asymmetric domains than those discussed here (or curved triple-lines). This gives us some confidence that we have compared the most favoured tricontinuous patterns for balanced structures. (We hasten to add that the situation for unbalanced structures, with a preferred curvature of the triple-line to accommodate the volume differences between domains, is far more complex, and likely to involve other structures, including patterns with distinct labyrinth graphs.)

An arresting aspect of three-arm polyphile assembly is the possibility of formation of chiral mesophases in the absence of chiral molecular constituents: the promotion of chirality can be theoretically achieved by splayed three-arm molecules that need not be chiral. For example, if the arms radiate from three positions on a central aromatic (e.g. benzene) core, the resulting polyphiles are themselves achiral; were those arms to be engineered to exhibit significant splay, our estimates of relative packing energies suggest that the 3qtz(145) (or, less likely, srs(24)) chiral mesostructures may form. This phenomenon is akin to that of ferroelectric chiral mesophases in achiral 'banana-shaped' mesogens, that have elicited significant interest among liquid crystal researchers.^{49,50} We are currently exploring this possibility with our achiral star polyphile molecules.

This paper has focused on three-arm star polyphilic self-assemblies, whose three moieties will, we believe, favour formation of tricontinuous structures. It is worth noting, however, that the patterns explored here are also likely to be found in more conventional amphiphilic systems, since their curvature homogeneity mimics in some respects that of their bicontinuous analogues, and can be ranked by orbifold areas, as above. In that

respect, we are encouraged by the recent report of the 3etc(187) pattern in a mesoporous silica material,³ that suggests these patterns are indeed more generally relevant.

9 Acknowledgements

We thank Alan Schoen for correspondence related to minimal surfaces and Michael O'Keeffe for discussions on triple intergrowths of nets. STH and CO also thank the organisers of the Foams and Minimal Surfaces Workshop at the Isaac Newton Institute for Mathematical Sciences for the opportunity to initiate this work. SH acknowledges the Australian Research Council for a Federation Fellowship.

References

- 1 V. Alfredsson and M. Anderson, *Chem. Mater.*, 1996, **8**, 1141–1146.
- 2 C. Gao, Y. Sakamoto, K. Sakamoto, O. Terasaki and S. Che, *Angew. Chem., Int. Ed.*, 2006, **45**, 4295.
- 3 Y. Han, D. Zhang, L. L. Chng, J. Sun, L. Zhao, X. Zou and J. Y. Ying, *Nature Chem.*, 2009, **1**, 123.
- 4 S. T. Hyde and S. Ramsden, *Europhys. Lett.*, 2000, **50**, 135–141.
- 5 S. Hyde and C. Oguey, *Eur. Phys. J. B*, 2000, **16**, 613–630.
- 6 S. Hyde and G. Schroeder, *Curr. Opin. Colloid Interface Sci.*, 2003, **8**, 5.
- 7 S. Okamoto, H. Hasegawa, T. Hashimoto, T. Fujimoto, H. Zhang, T. Kazama, A. Takano and Y. Isono, *Polymer*, 1997, **38**, 5275.
- 8 S. Sioula, N. Hadjichristidis and E. Thomas, *Macromolecules*, 1998, **31**(23), 8429–8432.
- 9 S. Sioula, N. Hadjichristidis and E. Thomas, *Macromolecules*, 1998, **31**(16), 5272–5277.
- 10 A. Zioga, S. Sioula and N. Hadjichristidis, *Macromol. Symp.*, 2000, **157**, 239.
- 11 K. Yamauchi, S. Akasaka, H. Hasegawa, H. Iatrou and N. Hadjichristidis, *Macromolecules*, 2005, **38**(19), 8022–8027.
- 12 A. Takano, W. Kawashima, S. Wada, K. Hayashida, S. Sato, S. Kawahara, Y. Isono, M. Makihara, N. Tanaka, D. Kawaguchi and Y. Matsushita, *J. Polym. Sci., Part B: Polym. Phys.*, 2007, **45**(16), 2277.
- 13 A. Takano, S. Wada, S. Sato, T. Araki, K. Hirahara, T. Kazama, S. Kawahara, Y. Isono, A. Ohno, N. Tanaka and Y. Matsushita, *Macromolecules*, 2004, **37**(26), 9941–9946.
- 14 K. Hayashida, W. Kawashima, A. Takano, Y. Shinohara, Y. Amemiya, Y. Nozue and Y. Matsushita, *Macromolecules*, 2006, **39**(14), 4869–4872.
- 15 K. Yamauchi, K. Takahashi, H. Hasegawa, H. Iatrou, N. Hadjichristidis, T. Kaneko, Y. Nishikawa, H. Jinnai, T. Matsui, H. Nishioka, M. Shimizu and H. Fukukawa, *Macromolecules*, 2003, **36**(19), 6962–6966.
- 16 K. Hayashida, A. Takano, S. Arai, Y. Shinohara, Y. Amemiya and Y. Matsushita, *Macromolecules*, 2006, **39**(26), 9402–9408.
- 17 K. Hayashida, N. Saito, S. Arai, A. Takano, N. Tanaka and Y. Matsushita, *Macromolecules*, 2007, **40**(10), 3695–3699.
- 18 P. Tang, F. Qiu, H. Zhang and Y. Yang, *J. Phys. Chem. B*, 2004, **108**(24), 8434–8438.
- 19 A. Takano, W. Kawashima, A. Noro, Y. Isono, N. Tanaka, T. Dotera and Y. Matsushita, *J. Polym. Sci., Part B: Polym. Phys.*, 2005, **43**(18), 2427.
- 20 T. Dotera and A. Hatano, *J. Chem. Phys.*, 1996, **105**, 8413.
- 21 T. Gemma, A. Hatano and T. Dotera, *Macromolecules*, 2002, **35**, 3225–3227.
- 22 Y. Bohbot-Raviv and Z.-G. Wang, *Phys. Rev. Lett.*, 2000, **85**, 3428–3431.
- 23 T. Dotera and T. Gemma, *Philos. Mag.*, 2006, **86**, 1085.
- 24 C.-I. Huang, H.-K. Fang and C.-H. Lin, *Phys. Rev. E: Stat., Nonlinear, Soft Matter Phys.*, 2008, **77**, 031804.
- 25 L. de Campo, M. Moghaddam, and S. T. Hyde, in preparation, 2009.
- 26 H. J. Limbach, A. Arnold, B. A. Mann and C. Holm, *Comput. Phys. Commun.*, 2006, **174**(9), 704.
- 27 J. Kirkensgaard and S. T. Hyde, in preparation, 2009.
- 28 J. Kirkensgaard and S. T. Hyde, *Phys. Chem. Chem. Phys.*, 2009, **11**, 2016.

-
- 29 K. Brakke, *Exp. Math.*, 1992, **1**, 141–165.
- 30 K. Brakke, *Evolver*, <http://www.susqu.edu/brakke/evolver/>.
- 31 R. Phelan, D. Weaire and K. Brakke, *Exp. Math.*, 1995, **1**, 181–192.
- 32 E. A. Lord and A. L. Mackay, *Current Sci.*, 2003, **85**, 346–362.
- 33 S. T. Hyde and C. Oguey, in preparation, 2009.
- 34 X. Zeng, G. Ungar and M. Impéror-Clerc, *Nat. Mater.*, 2005, **4**, 562.
- 35 S. Hyde, S. Andersson, Z. Blum, S. Lidin, K. Larsson, T. Landh, and B. Ninham, *The Language of Shape*, Elsevier Science, Amsterdam, 1997.
- 36 W. Fischer and E. Koch, *Philos. Trans. R. Soc. London, Ser. A*, 1996, **354**, 2105.
- 37 M. O’Keeffe, M. A. Peskov, S. Ramsden and O. M. Yaghi, *Acc. Chem. Res.*, 2008, **41**, 1782–1789; <http://rcsr.anu.edu.au>.
- 38 G. E. Schröder-Turk, A. Fogden and S. T. Hyde, *Eur. Phys. J. B*, 2006, **54**, 509–524.
- 39 S. Hyde, in *Foams and Emulsions*, ed. J.-F. Sadoc and N. Rivier, Addison-Wesley, Dordrecht, The Netherlands, 1999, pp. 427–470.
- 40 C. Bonneau, O. Delgado-Friedrichs, M. O’Keeffe and O. M. Yaghi, *Acta Crystallogr., Sect. A: Found. Crystallogr.*, 2004, **60**, 517.
- 41 J. Middleton, H. Averdunk and A. Sheppard, *Mango*, <http://xct.anu.edu.au/mango/>.
- 42 A. Wells, *Three-dimensional nets and polyhedra*, John Wiley and Sons, New York, 1977.
- 43 V. Elser, *Philos. Trans. R. Soc. London, Ser. A*, 1996, **354**, 2071–2075.
- 44 W. Helfrich, *Z. Naturforsch., C: Biochem., Biophys., Biol., Virol.*, 1973, **28**, 693.
- 45 A. Goetz, *Introduction to Differential Geometry*, Addison-Wesley, Reading, Massachusetts, 1970, p. 229.
- 46 A. Goetz, *Introduction to Differential Geometry*, Addison-Wesley, Reading, Massachusetts, 1970, p. 307.
- 47 S. Hyde, K. Larsson, Z. Blum, T. Landh, S. Lidin, B. Ninham, and S. Andersson, *The Language of Shape*, Elsevier Science, Amsterdam, 1986.
- 48 S. T. Hyde and S. Ramsden, *Eur. Phys. J. B*, 2003, **31**, 273–284.
- 49 T. Niori, T. Sekine, J. Wanatabe, T. Furukawa and H. Takezoe, *J. Mater. Chem.*, 1996, **6**, 1231.
- 50 D. Link, G. Natale, R. Shao, J. MacLennan, N. Clark, E. Kšrblova and D. Walba, *Science*, 1997, **278**, 1924–1927.